Archives of Civil and Mechanical Engineering (2022) 22:85
https://doi.org/10.1007/s43452-022-00397-6

ORIGINAL ARTICLE

Performance and microstructure analysis of high-strength concrete incorporated with nanoparticles subjected to high temperatures and actual fires

D. E. Tobbala[1] · A. S. Rashed[2,3] · Bassam A. Tayeh[4] · Tamer I. Ahmed[5]

Received: 19 October 2021 / Revised: 21 January 2022 / Accepted: 13 February 2022 / Published online: 4 March 2022
© Wroclaw University of Science and Technology 2022

Abstract
Currently, nanoparticles are used as admixtures to reduce the thermal deterioration of concrete after exposure to fire. However, the influence of high temperature on high-strength concrete (HSC) containing silica fume and nanoparticles has not been investigated well. In this study, various HSC mixes incorporated with 1%, 2%, 3% and 4% nanosilica (NS) or 1% and 2% nanoferrite (NF) were prepared to produce HSC with high enduring strength after being subjected to high temperatures of up to 800 °C and actual fires. The specimens were assessed via scanning electron microscopy, compression and splitting tensile tests, modulus of elasticity test, and water permeability coefficient analysis. Results showed that using NS and NF percentages of up to 3% and 2%, respectively, in HSC improved the mechanical properties and water permeability coefficient at elevated temperatures. The compressive strength of the heated specimens with 3% NS was better than those with 2% NF at temperatures 200 °C–800 °C. With regard to the microstructure feature, the results confirmed that NS acted as an adequate filling material, which produced a condensed microstructure with extra compressed hydration outputs. This may be associated to higher pozzolanic reaction of NS with high distribution that formed additional calcium silicate hydrate gel. The specimens with 3% NS had no cracks until the temperature of 800 °C, but their porosity increased slightly.

Keywords Nanosilica · Fire · High temperature · Mechanical properties · Microstructure

1 Introduction

Nanosilica (NS) and nanoferrite (NF) have elicited the most interest amongst all nanomaterials used to improve the properties of concrete [1]. This interest may be due to their higher reactivity compared to other nanomaterials [2, 3]. NS and NF serve as a nanofiller material stuffing the pores between calcium silicate hydrate (CSH) gel particles and refining the microstructure [4–7]. NS has a high pozzolanic activity and reacts with calcium hydroxide (CH), thus generating abundant CSH, resulting in a condensed cement matrix and increasing concrete strength and durability [8]. On the other hand, NF has a physical effect, and it operates as nuclei to speed up the hydration process of the cementitious material to produce CSH; it also reacts with CH and forms calcium ferric hydrate (CFH) gel [9]. The addition of a small amount (up to 3%) of either NS or NF enhances the bonding between the hardened cement paste (CP) matrix and aggregates in the interfacial transition zone (ITZ) [10]. Many researchers have comprehensively investigated their influence on the hardening properties of concrete. Sumesh et al. [11] examined the effects of nanoparticles on the hardening, durability and bonding properties of cement mortar and geopolymer paste and reported that the use of nanomaterials with effective particle sizes increases the efficiency and strength of cement mortar. Li et al. [12]

✉ Bassam A. Tayeh
btayeh@iugaza.edu.ps

1 Department of Civil and Architecture Construction, Suez University, Suez, Egypt

2 Department of Physics and Engineering Mathematics, Faculty of Engineering, Zagazig University, Zagazig, Egypt

3 Faculty of Engineering, Delta University for Science and Technology, Gamasa, Egypt

4 Department of Civil Engineering, Faculty of Engineering, Islamic University of Gaza, P.O. Box 108, Gaza Strip, Palestine

5 Department of Civil Engineering, Higher Institute of Engineering and Technology in Kafr-Elsheikh, Kafr-Elsheikh, Egypt

reported that the addition of nanoparticles can improve the mechanical characteristics of concrete. Furthermore, concrete containing nano-TiO_2 has better abrasion resistance compared with concrete with an equivalent amount of nano-SiO_2 [13]. With the advancement of nanotechnology, SiO_2 can now be produced in nano-sized particles with predictable size ranges. The effect of the size of SiO_2 elements on concrete strength was investigated by Schoepfer and Maji [14]. Compressive strength tests revealed a significant increase in strength when particle size of SiO_2 is reduced to 12 nm. Researchers have been working to enhance the durability and long-term sustainability of concrete, and considerable improvement in the mechanical characteristics of cementitious materials has been achieved through the integration of nanoparticles [15, 16]. Nano-modification may be used to develop a cementitious material that is highly durable, strong and environmentally friendly [17]. Nanoparticles can reduce cement use and convert cement-based goods into electric/thermal sensors or crack-repairing materials because of their reinforcing action [18, 19]. The addition of ultrafine nano-elements aids in the reduction of cement content by moderately substituting cement by weight ground to increase the binding impact [7, 17, 20]. Ultrafine nanomaterial particles also help reduce micropore development by serving as a filler agent, resulting in highly dense concrete that automatically limits micropore growth in ultrahigh-strength concrete (UHSC) structures [21, 22]. Previous studies demonstrate that nano-silica can improve concrete's resistance to high temperatures, along with increase in the mechanical properties of high-strength concrete at high temperatures [23, 24]. The presence of nanosilica in mixtures increases resistance to elevated temperatures that is evident as the concrete, after exposure to elevated temperatures maintain most of its compressive strength (f_c). Inclusion of Nano silica also helps reduce crack length compared with plain or even blended mixtures containing other supplementary materials [25, 26]. At temperatures of 200 °C to 400 °C, abundant CSH is produced as a result of the high pozzolanic activity of nanosilica, and anhydrous cement grains are hydrated during the internal autoclaving process [27, 28]. Moreover, the pore size distribution in the matrix at high temperatures is reduced by increasing the nanosilica content [29]. The resistance of concrete to elevated temperatures of up to 400 °C can be enhanced by increasing the nanosilica content, but an opposite effect occurs at temperatures exceeding 400 °C [30, 31]. Furthermore, the incorporation of NS delays the deterioration of fired concrete by reducing the thermal conductivity of concrete [32]. This condition implies that long exposure to fire is essential to attain the required temperature at the core of the concrete members. Thus, the thermal degradation of blended concrete members is delayed [33]. Spinel $ZnFe_2O_4$ nanoparticles formulated via the sol–gel process (17.5 nm) have also been added with different doses of up to 2% to boost the physico-mechanical and fire resistivity of hardened cement pastes. The optimum addition is 1% $ZnFe_2O_4$ [34].

The previous studies focused only on studying the effects of elevated temperature without analysing real fire situations. Moreover, the literature didn't provide any design and relative cost estimation for a concrete structure incorporating nanoparticles. For the previous issues, the recent study aims to achieve three objectives. The first is to examine the effect of elevated temperature of silica fume (SF) on high-strength concrete incorporated with NS or NF under elevated temperatures up to 800 °C. The second aim is to investigate the fire resistance of specimens subjected to 600 °C heat under an initial cracking load of control mix for one hour. The third is to make a cost estimation for designing reinforced concrete columns using every mix. Nine mixes were prepared to study the effect of adding different percentages of NS and NF. Their results were compared with those of common and SF concrete mixes. Moreover, the effect of increasing the cement content of 3% NS concrete to 450 kg/m^3 was studied for comparison. Compressive strength (f_c), splitting tensile strength (f_t) and modulus of elasticity (E_c) were investigated at room temperature. The SEM analysis of the specimens was performed to explain the obtained results and compare it with works of El-Enein et al. and Nili et al. [35, 36]

2 Experimental work

2.1 Materials and mix proportion

Nanosilica (NS) was prepared from rice husk by using hot hydrochloric acid via chemical treatment and burning [37]. After this treatment, an amorphous powder with 100% purity and an average particle size of 6.25 nm was obtained. $CoFe_2O_4$ nanoparticles (NF) were prepared through the citrate-gel method [9] with average particle size 29.62 nm and 100% purity. Physical and chemical characterisations of the used nanofillers were performed. Type I ordinary Portland cement (OPC type I 52.5 N) and SF were utilised as binders in the mixes, as shown in Table 1. The main characteristics of the NS sample were measured using an X-ray diffraction (XRD) apparatus, an energy-dispersive X-ray (EDX) spectroscopy device and a transmission electron microscopy (TEM) instrument, as shown in Fig. 1. Cement was tested in accordance with ASTM C143M-15a [38]. Natural sand and dolomite were used as fine and coarse aggregates with specific gravities of 2.67and 2.75 and volume weights of 1.66 and 1.78 t/m^3, respectively. The fineness modulus of sand was 2.82, and the NMZ and water absorption of dolomite were 12.5 mm and 1.1%, respectively. The aggregate tests

Table 1 Chemical composition and physical properties of OPC, SF, NS and NF

Items	OPC	SF	NS	NF
Chemical composition (wt%)				
SiO_2	20	97.20	100	0
Al_2O_3	6.25	0.25	–	–
Fe_2O_3	3.55	0.54	–	–
$CoFe_2O_4$	–	–	–	100
CaO	62.34	0.21	–	–
MgO	2.12	0.43	–	–
SO_3	2.42	0.11	–	–
LOI	1.67	0.74	–	–
K_2O	0.75	0.45	–	–
Na_2O	0.81	0.15	–	–
Physical properties				
Specific gravity	3.15	2.15	2.0	5.3
Avg. particle size (nm)	21,000	1000	6.25	29.62

were performed in accordance with ASTM C33/C33M–18 [39]. In order to achieve good workability of mixes and even distribution of NS in the concrete mix, Sika Visco-Crete 5–930 with a density of 1.08 kg/m^3 was used as the super-plasticizer (SP) in accordance with ASTM-C-494 types G and F.

Table 2 shows the preparation of the nine concrete mixes. The binder (B) involved cement content (C), SF, NS and NF. The cement content and the percentages of sand (S), aggregates (Agg), water (W) and super-plasticizer (SP) "S/Agg, W/B and SP/B" were kept constant in all the mixes at 400 kg/m^3 and 40%, 30% and 4%, respectively. Uniform dispersion of NS and NF in the mixes was not easy because of their high surface energy and low content in the mixture. All these mixes containing NS (1–4%) and NF (1–2%) were prepared according to the following procedure. First, the Nanoparticles were stirred in water separately in a small mixer at a speed of 120 rpm for 2 min. Next, cement, silica

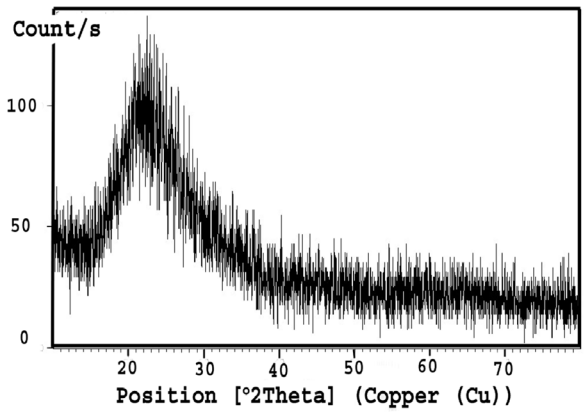

(a) X-Ray Diffraction (XRD) Analysis

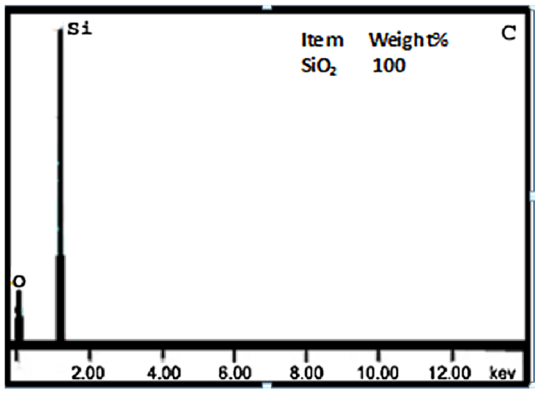

(b) Energy Dispersive X-Ray (EDX) Analysis

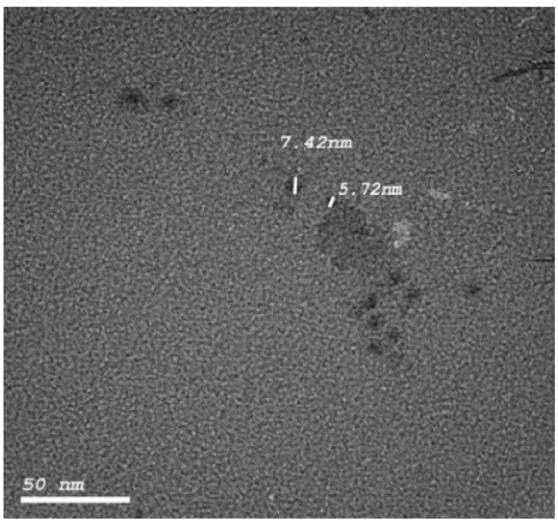

(c) Transmission electron microscopy (TEM) Analysis

Fig. 1 Characterisation of the NS sample [37]

Table 2 Proportions of the designed mixes and their cost ratio with respect to the M_O mix

Mix no	Proportions of mixes (kg/m^3)								(Cost/ m^3) / M_o
	OPC	SF	NS	NF	S	D	W	SP	
M_o	400	0	0	0	792.3	1188.4	120	16.0	1.00
M_{SF}	400	60	0	0	740.8	1111.2	138.0	18.4	1.269
M_{NS1}	400	60	4	0	737.2	1105.8	139.2	18.6	1.7322
M_{NF1}	400	60	0	4	737.2	1105.8	139.2	18.6	2.197
M_{NS2}	400	60	8	0	733.6	1100.5	140.4	18.7	2.657
M_{NF2}	400	60	0	8	733.6	1100.5	140.4	18.7	3.123
M_{NS3}	400	60	12	0	730.1	1095.1	141.6	18.9	2.66
M_{NS4}	400	60	16	0	726.5	1089.7	142.8	19.0	3.12
M_{450}	450	67.5	13.5	0	687.3	1031.0	159.3	21.2	3.26
Cost of component / OPC	1	5	200	1000	0.051	0.093	0	75	

where's * the content of the Table were in (kg/m^3)

OPC cement content (OPC I-52.5 N), *W* water, *SF* silica fume, *D* dolomite as a coarse aggregate, *NS* nano-silica, *S* sand as a fine aggregate, *NF* nano-ferrite, *SP* super plasticizer, (Cost/ m^3) / M_O: cost of 1 m^3 ratio with respect to M_O mix, cost of component/OPC: cost of component with respect to local OPC cost (Steel / cement) cost ratio was 13

fume, sand and dolomite were dry mixed at medium speed of 80 rpm for 1 min. Afterwards, keeping the mixer at medium speed, about two thirds of water with nanoparticle was added gradually to the dry constituents for about 30 s. SP was added to the rest of the third mixing water and added gradually while mixing for another 30 s. Finally, the mixture was rested for 30 s and then remixed for 1 min [37]. The specimens were demoulded after 24 h of casting and alleviated in a water tank at ambient temperature until the test dates.

2.2 Specimens and testing

2.2.1 Specimens

Nine mixes were designed as illustrated in Table 2. For each mix, three cubes of dimensions 100 × 100 × 100 mm were prepared for each of the six curing ages to test for compressive strength. Three cylindrical specimens of height 300 mm and diameter of 150 mm were cast for each mix to test modulus of elasticity and tensile strength. For water permeability test, three cylindrical specimens of height 150 mm and diameter of 150 mm for each mix.

2.2.2 Mechanical and physical testing

A compression test was performed after 7–180 days of aging by using 100 × 100 × 100 mm cubes. The test was carried out in accordance with BS 1881–116: 1983. A splitting tensile test was performed on the 28th day by using 150 × 300 mm cylinders and carried out in accordance with BS 1881–117: 1983. Static modulus of elasticity (E) compression was applied on the 28th day by using 150 × 300 mm cylinders and carried out in accordance with ASTM C469-65 (1975). A water permeability test was conducted on the 28th day. For a five-hour period, the concrete specimens were subjected to a hydrostatic water flow of 30 bars. The permeability coefficient (K) was calculated based on Darcy's law.

2.2.3 Durability testing

The durability of concrete mixes was investigated through high elevated temperature testing and actual fire exposure. For elevated temperature, the specimens were heated in an electric furnace at fixed temperatures with exposure time of for 2 h. The volume of electrical furnace was of (250 × 400 × 350) mm with heating rate of 20 °C /min and maximum achievable temperature of 1200 °C. The heated specimens were left to cool down at ambient temperature until it reaches room temperature as shown in Fig. 2 [23]. A fire test was carried out using 100 × 100 × 100 mm cubes. Two German thermocouples (type J) were fixed during the casting of the cubes. The first was imbedded in the middle of a cube to measure the inner temperature, and the other was fixed on the surface of the cube to measure the surface temperature. The cubes were cured for 28 days, removed from the curing tank and allowed to dry at ambient temperature for about 7 days before testing. The fire test was conducted whenever the specimens were loaded with the initial cracking load in accordance with ASTM E119 [40]. The firing tool was designed according to the standard fire test curves of ASTM-E119, and its time–temperature relation was compatible with ISO 834–11. All specimens were loaded with a constant load of 70 KN representing the initial

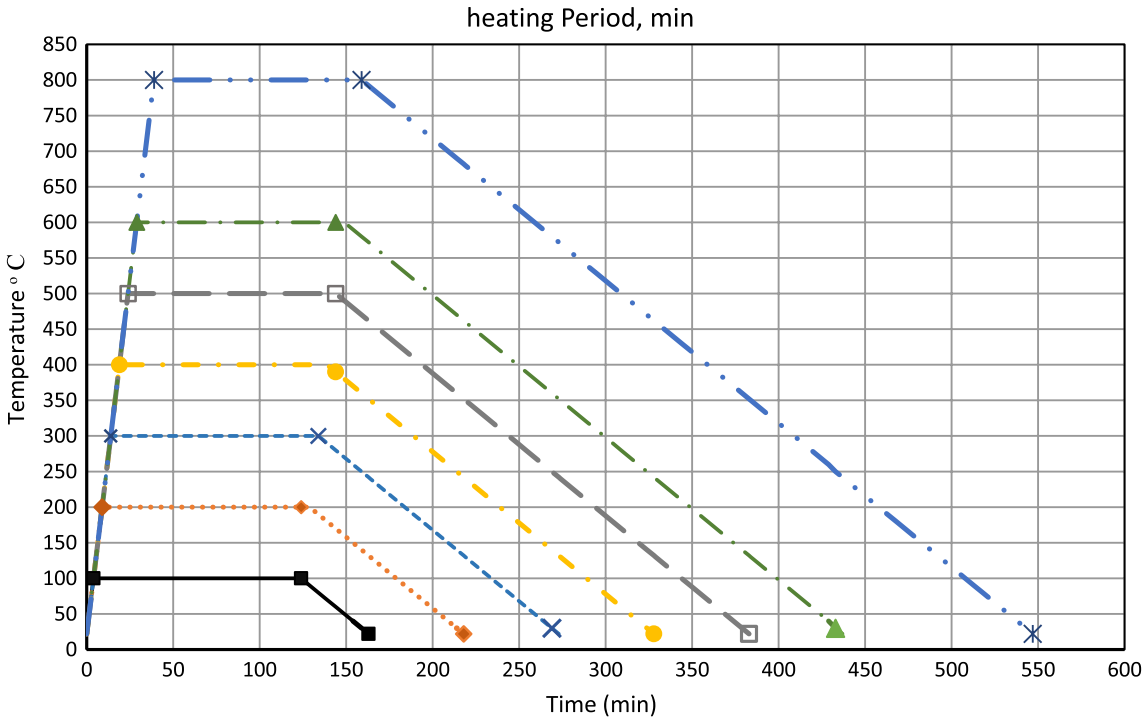

Fig. 2 Heating period of specimens per min

crack load of the control mix. Each specimen was loaded using a hydraulic jack machine with a capacity 10,000 psi, an accuracy of 100 psi and a radius of 98 mm. Each specimen was inserted inside the firing tool. The thermocouples were connected to a voltmeter to measure the output voltage, which was converted into temperature in Celsius throughout the thermocouple curve. Firstly, each specimen was loaded with the predetermined load (70 KN) and kept constant during firing. Secondly, the temperature was raised to 600 °C on the surface of the cube at a rate of 50 °C/min then maintained at 600 °C for an hour under loading. Lastly, the fire was extinguished, and the load on the specimen was gradually increased until failure occurred. The f_c value was recorded, as shown in Fig. 3.

Fig. 3 Firing of a loaded specimen

2.2.4 SEM analysis

Samples for SEM analysis were taken from the centre of cubes, grinded and adhered on aluminium stub using adhesive carbon tape. Samples were sputter coated with gold for 1 min. Then, examination was performed using SEM (JEOL, JSM IT-100) at 20 kv.

The heated specimens were exposed to various temperatures (100 °C—800 °C) for all mixes after curing for 28 days.

2.2.5 Cost estimation of concrete column

An economic assessment of one cubic meter of the concrete mixes was performed and the cost of the materials was obtained from the seller's reports. The following formula was used based on the seller's reports.

$$\begin{aligned}\text{Cost}_i = &\left(1 \times \text{C}_i\right) + \left(5 \times SF_i\right) + \left(200 \times NS_i\right) \\ &+ \left(1000 \times NF_i\right) + \left(0.00225 \times W_i\right) \\ &+ \left(0.051 \times S_i\right) + \left(0.093 \times D_i\right) + \left(75 \times SP_i\right)\end{aligned} \quad (1)$$

where Cost_i is the cost of 1 m^3 of produced concrete blend i, C_i is the cement content of blend i, SF_i is the SF content, NS_i is the NS content, NF_i is the NF content, W_i is the water content, S_i is the sand content, D_i is the dolomite content and SP_i is the SP content. All of the components of concrete mix i were measured in kg/m^3.

Moreover, an economic assessment of the designed column of concrete mixes was performed. The cost of the reinforced column of mix i was evaluated by assuming a load of 10,000 KN. The quality control of nanoparticle concrete mixes must be excellent. Thus, the confidence percentage and coefficient of variance (V %) were assumed to be 95% and 5%, respectively. The designed compressive strength (f_{cu}) of mix i at 28 days of age was calculated with Eq. 2 and designed area of the concrete and the area of the steel column were calculated with Eq. 3 where α_i was derived from Eq. 4. The β_i and the factor of safety of concrete (γ_c) and steel (γ_c) were taken as 0.67, 1.75 and 1.36. The yield strength of steel (f_y) and the density of steel D_{st}) were 400 MPa and 7.8 ton/ m^3, respectively. The variable parameters in Eqs. (2)–(5) are tabulated in Table 3.

$$(f_{cu})_{i=}(f_m)_i * (1 - 1.67 * V) \quad (2)$$

$$P_u = 0.9*\left(\alpha_i\beta_i\frac{(f_{cu})_i}{\gamma_c}\text{A}_{ci} + \frac{f_y}{\gamma_s}\,\text{A}_{si}\right) \quad (3)$$

where

$$\left[\alpha_i = 0.85 - 0.0033\left(f_{cu} - 60\right)\right] \geq 0.67 \quad (4)$$

$$Cost_{col\,i} = \left(cost_i * A_{ci} + A_{si} *_{st} *\ 10^3 * cost_{st}\right) * h^{-6}_{col*10} \quad (5)$$

3 Results and discussion

3.1 Fresh properties

Figure 4 shows the fresh and hard densities of the SF concrete mixes prepared with the incorporation of nanoparticles particles in comparison with the density of the control mix. The figure indicates that the fresh density of the SF concrete mixes incorporated with nanoparticles was less than that of the control mix due to their lesser specific gravity. Meanwhile, the dry density of all the mixes was greater than that of the control mix due to the high density of the matrix resulting from the highly pozzolanic reaction of NS and the physical role of NF. Both, NS and NF worked as a catalyst for cement hydration and SF pozzolanic manner, thereby producing highly dense concrete [9].

3.2 Water permeability

Figure 5 shows that the water permeability coefficients (K) of M_o and M_{SF} mixes were 4.04×10^{-11} and 1.65×10^{-11} cm/sec, respectively. Permeability when

Table 3 Analysis of studied axially loaded short column

Mix	f_{mean}	f_{cu}	α	β	A_C (mm^2)	A_S (mm^2)	R%	(Cost of col/ M_{O}) %
M_O	55.5	50.4	0.83	0.67	574,432.1	5744.321	100.0	100.0
M_{SF}	71.9	66.0	0.80	0.67	464,527.9	4645.279	80.9	84.1
M_{NS1}	83.3	76.5	0.81	0.67	423,414.3	4234.143	73.7	81.6
M_{NF1}	80.0	73.4	0.76	0.67	434,282.7	4342.827	75.6	88.9
M_{NS2}	93.5	85.8	0.76	0.67	395,889.8	3958.898	68.9	85.7
M_{NF2}	95.6	87.8	0.74	0.67	390,823.8	3908.238	68.0	89.3
M_{NS3}	100.4	92.2	0.73	0.67	380,585.6	3805.856	66.3	82.4
M_{NS4}	104.6	96.0	0.74	0.67	372,657.1	3726.571	64.9	85.1
M_{450}	102.3	93.9	0.83	0.67	376,939.7	3769.397	65.6	87.4

where f_{mean}: mean compressive strength at 28 days age, f_{cu}: characteristic compressive strength,$\boldsymbol{\alpha}$: factor to substitute slow loading, $\boldsymbol{\beta}$: factor to transfer from cube to cylinder, A_C: cross section of designed column, A_S: area of steel of designed column (0.01 A_C), R%: area of concrete and steel of designed column percentage with respect to M_O, (Cost/ col) / M_O: cost percentage of designed column with respect to M_O mix under constant design load 10,000 ton

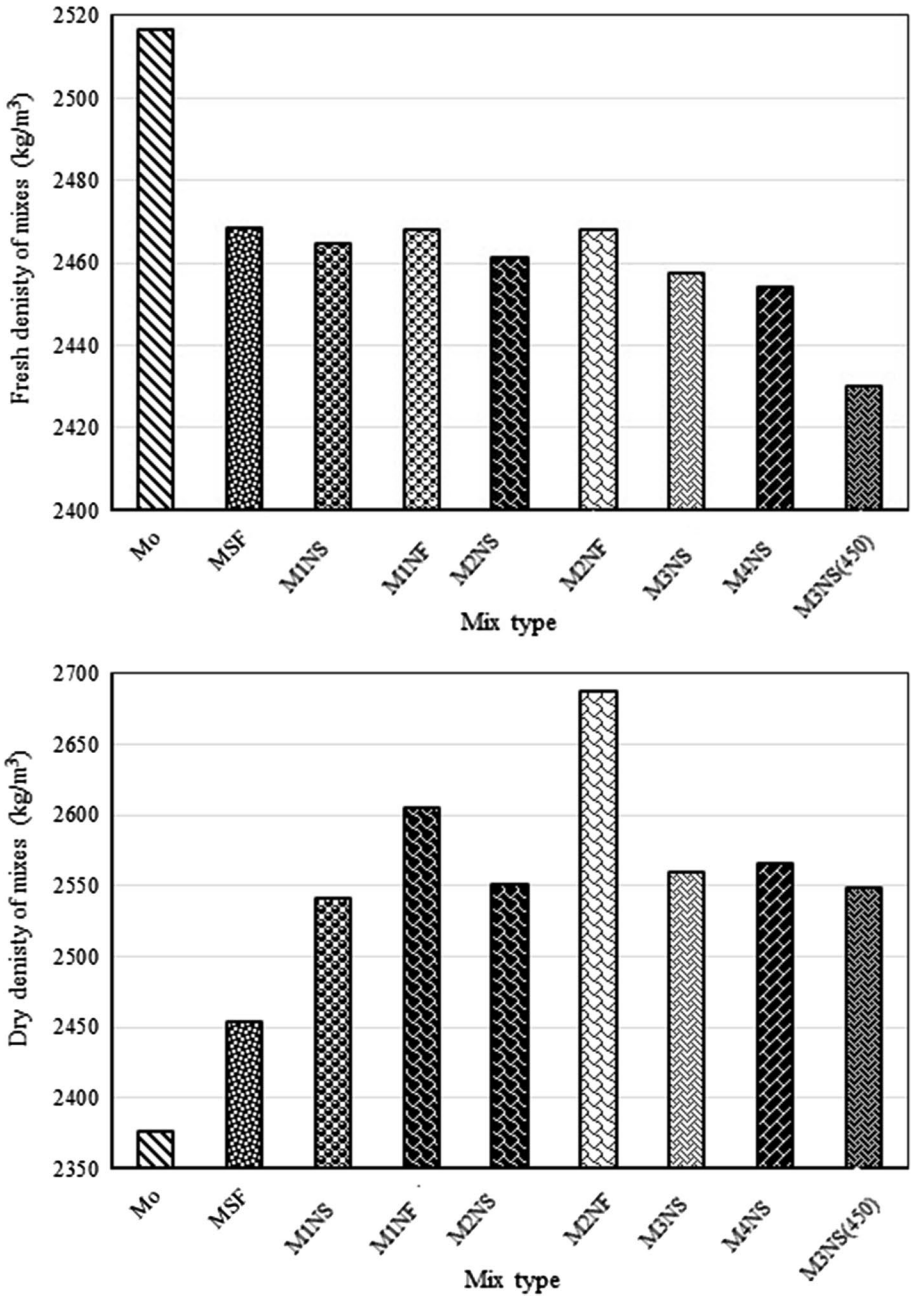

Fig. 4 Fresh and dry density of concrete mixes

the NS content was increased up to 4% was found to be $0.458 \times 10–11$ cm/sec. The K of M_{450} was greater than that of $M_{NS4,}$ which means that there is no need to increase the cement content of NS mixes over 400 kg/m^3. The compressive strength of the MNS4 mix was better than that of the M450 mix, consequently, confirming the previous result that 4% NS is the best percentage. In addition, the K of 1% NF was larger than that of 1% NS while the K of 2% NF was smaller than that of 2% NS.

3.3 Mechanical properties

3.3.1 Compressive strength

Figure 6 illustrates the f_c of the nine mixes at various ages between 7 and 180 days. Adding SF improved f_c up to 35%. Adding NS improved f_c by up to 4%. This result may be due to the tiny particle size, large surface area, high purity and high pozzolanic reaction of NS. For example, inclusion of NS resulted in enhancement of compressive

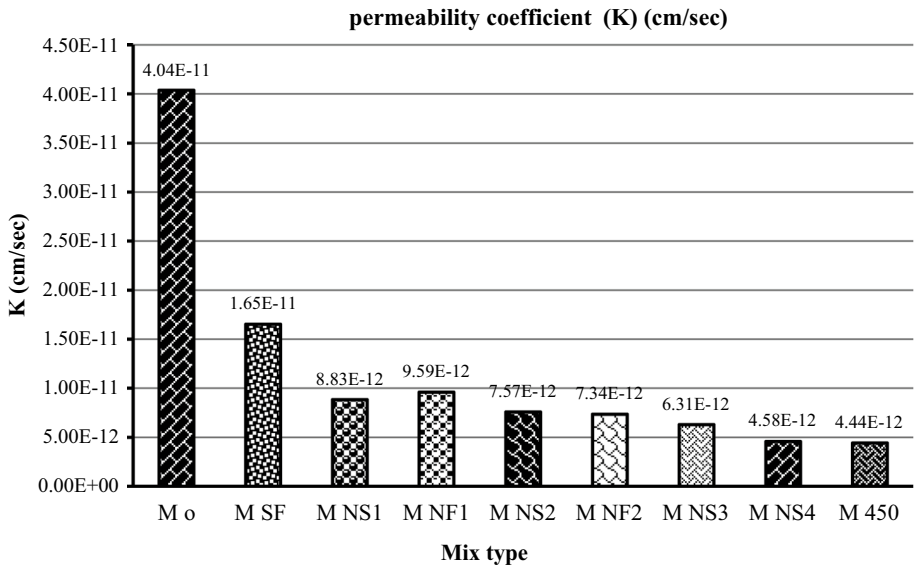

Fig. 5 Water permeability coefficient (K) (cm/sec) at 28 days of age

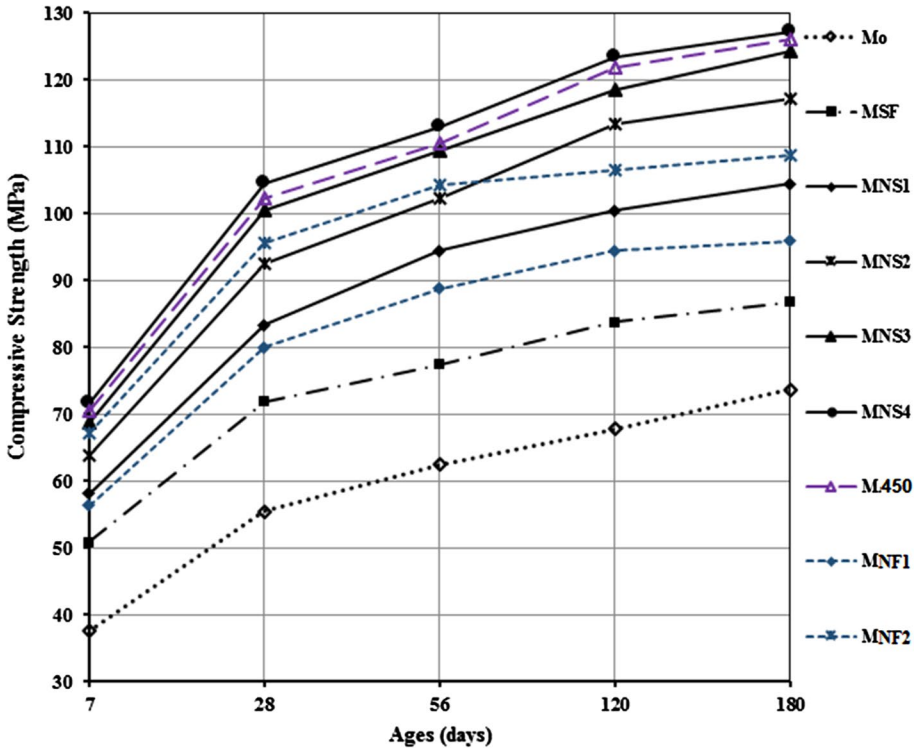

Fig. 6 Compressive strength of NS and NF mixes at 7–180 days of age at room temperature

strength by up to 89% and 73% at 28 and 180 days of age, respectively. Increasing of the cement content of the M_{NS3} mix from 400 kg/m^3 to 450 kg/m^3 required a proportional increment in SF, NS and SP. Hence, the cost of concrete increased by 11.1%. This increment in cement content improved the strength of M_{NS3} to 84% and 71% at 28 and 180 days of age, respectively. The improvement in strength is very small compared with the increase in cost. Moreover, increasing NS to up to 4% in M_{NS4} achieved better improvement with a very small increase in cost compared to the M_{450} mix. Meanwhile, adding 1% and 2% NF increased the improvement to 44.2% and 72.3% at 28 days of age and to 30.12% and 49.5% at 180 days of age, respectively. However, the f_c of M_{NF1} was smaller than that of M_{NS1} at all ages. The f_c of M_{NF2} was better than that of M_{NS2} at early ages up to 56 days of age. On the contrary, the f_c of M_{NF2} was smaller than that of M_{NS2} at late ages up to 180 days of age.

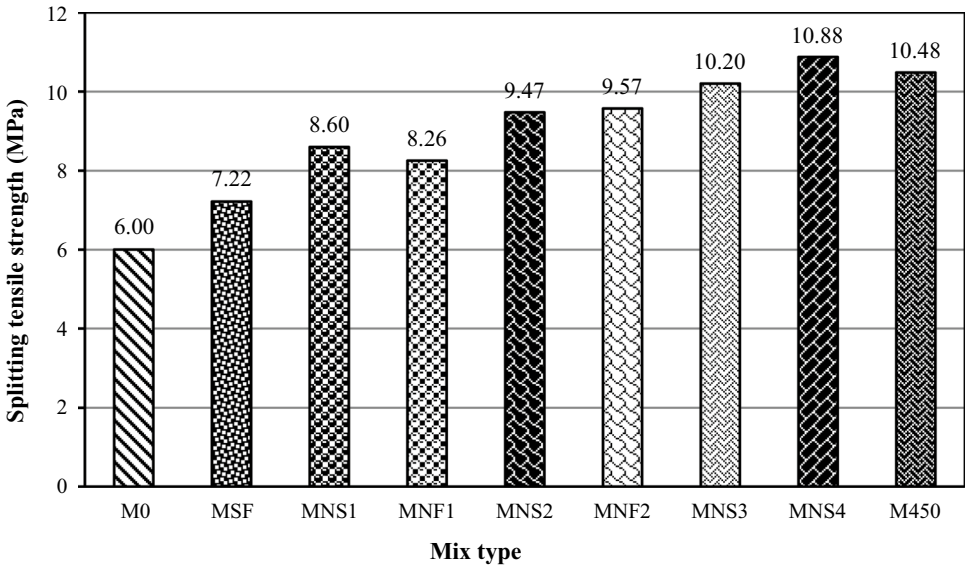

Fig. 7 Splitting tensile strength at 28 days of age

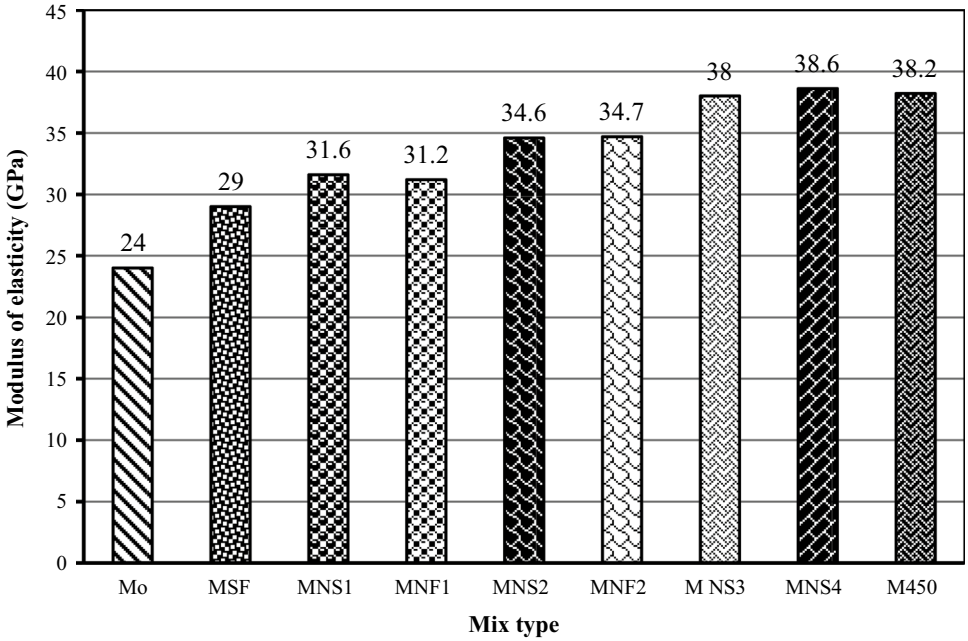

Fig. 8 Modulus of elasticity at 28 days of age

3.3.2 Splitting tensile and modulus of elasticity

Figures 7 and 8 show the splitting tensile strength (f_t) and modulus of elasticity (E_c) of the NS mixes at 28 days of age. Adding NS has enhanced the f_t and E_c by up to 81.3% and 60.8% respectively. Meanwhile, the incorporation of 1% and 2% NF improved f_t and E_c to 37.6% and 59.5%, respectively. Finally, increasing the cement content with 3% NS (M450) has enhanced the f_t and E_c by 74.6% and 59.2%, respectively. In conclusion, the results of MNF1 were smaller than those of MNS1. On the contrary, the results of MNF2 were better than those of MNS2, which agrees with the f_c results.

3.4 SEM of nano-specimens at room temperature

Figure 9 shows the SEM of the cement paste matrix (CP) and interfacial transition zone (ITZ) with the aggregate of the mixes at 28 days of age. Hydration outputs, such as CSH, ettringite and CH, were observed in the SF mix. Adding 2% NS produced a thick microstructure with extra-dense hydration products due to the highly pozzolanic reaction of NS with high distribution that formed an additional CSH gel. The microstructure improvement increased with increasing NS percentages of up to 4%. These results are in concurrence with the results of Abo El-Enein and Nili [35, 36] which in turn are also consistent with the other recent results. The

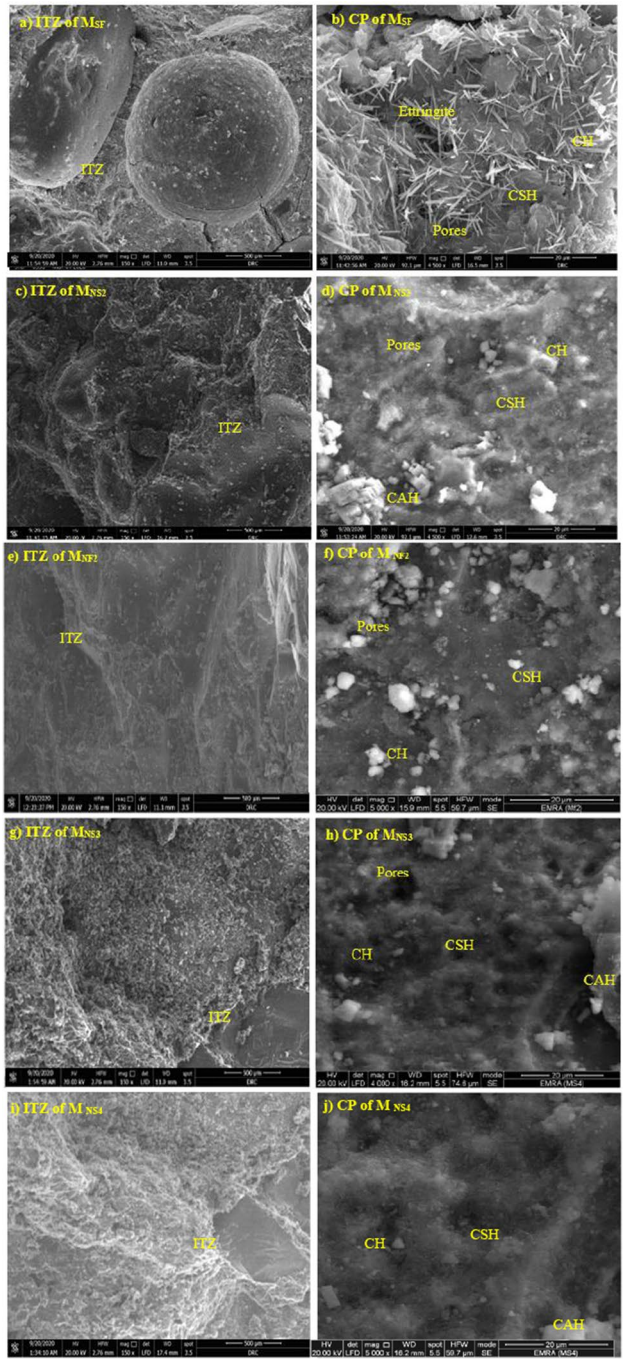

Fig. 9 SEM of ITZ and CP of the mixes at room temperature [9]

SEM analysis revealed that the M_{NS4} mix had the densest ITZ and contained the largest content of CSH gel combined with the lowest content of calcium aluminate hydrate (CAH) and traces of calcium hydroxide (CH).

The SEM CP and ITZ of M_{NF2} were better than those of M_{NS2} possibly because of the physical effect of NF, which acted as nuclei that accelerated the hydration process at the early ages [9].

3.5 Relative economic index

Figure 10 displays the relative economic index ratio (REI) of the mixes incorporated with nanoparticles with respect to the control mix. Clear increments were observed in 1 m3 of NS mixes from 1.73 up to 3.12. Furthermore, increasing the cement content to 450 kg/m3 has raised the REI to 3.26 without a significant increase in the mechanical properties or durability. And finally, the REI of NF mixes has increased up to 3.12. On the contrary, REI of the columns samples was reduced when compared to the 1 m3 ones (Fig. 10), which is due to the improvements in the compressive strengths of nano-particles mixes. For instance, the REI of the MNS4 column was 0.85, which improved fc to 1.885% at 28 days of age and reduced the area of the column to 0.65. Furthermore, the mechanical properties and REI of MNS4 mix were better than those of MNF2 mix. In conclusion, the MNS4 mix can be considered the most economical mix with the smallest relative area reduction amongst the other mixes.

3.6 Influence of temperature on compressive strength

Figure 11 shows the compressive strengths of the mixes with nano-particles subjected to different elevated temperatures (100 °C–800 °C) at 28 days. They were measured and compared with the f_c of M_o at the same temperatures. At 100 °C, the f_c of M_o and M_{SF} mixes has increased to 65 and 77.5 MPa, respectively. For instance, adding 4% NS has improved the f_c by up to 61.7%. These increments in strength were due to the accelerated hydration of the highly pozzolanic reaction of NS and cementitious materials. At 200° C, the strengths of M_O and M_{SF} have decreased to 60 and 69 MPa, respectively. The compressive strengths of the nano- particle mixes were also reduced but were still greater than the SF mix. For instance, adding 4% NS has improved the strength by up to 59.2%. At 400 °C, considerable reductions in the strengths of M_O and M_{SF} occurred and reached 40 and 36 MPa, respectively. Although the difference in strength between M_{NS3} and M_{NS4} mixes was small, the strength of mix M_{NS4} was still the highest up to exposure temperature of 400 °C, with the improvement reaching up to 104.3%. Moreover, at 600 °C, the strengths of M_o and M_{SF} became 20 and 16 MPa, respectively. The strength of the M_{NS3} mix was the highest, with the improvement reaching 232%. At 800 °C, the strength of the M_{NS3} mix was still the highest, with the improvement reaching 190%. Thus, the compressive strength values of M_{NS3} were the largest at 500 °C up to 800 °C. The f_c of M_{450} was smaller than that of M_{NS3} at all temperatures, and the difference between them increased with increasing temperature. Hence, increasing the cement content of SF concrete incorporated with NS had reverse effect on the concrete's resistance under high

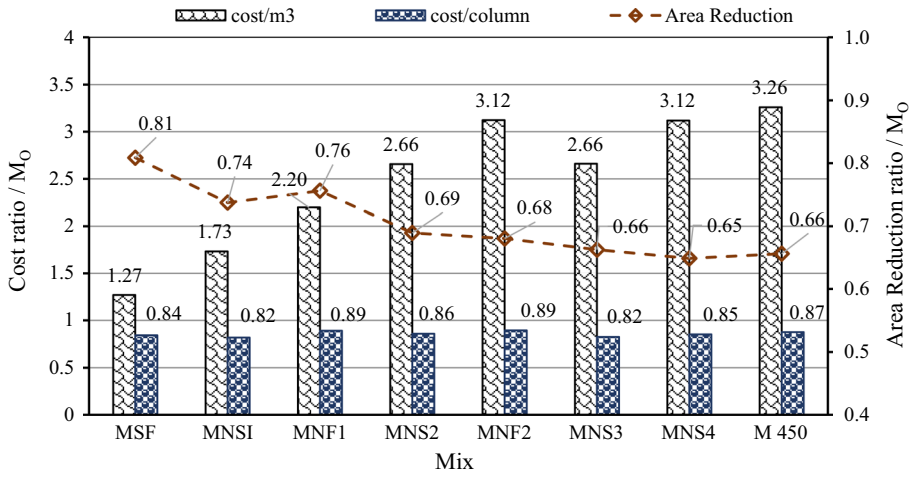

Fig. 10 Cross sec-area ratio and cost ratio of both of 1 m^3 and designed column relative to M_O

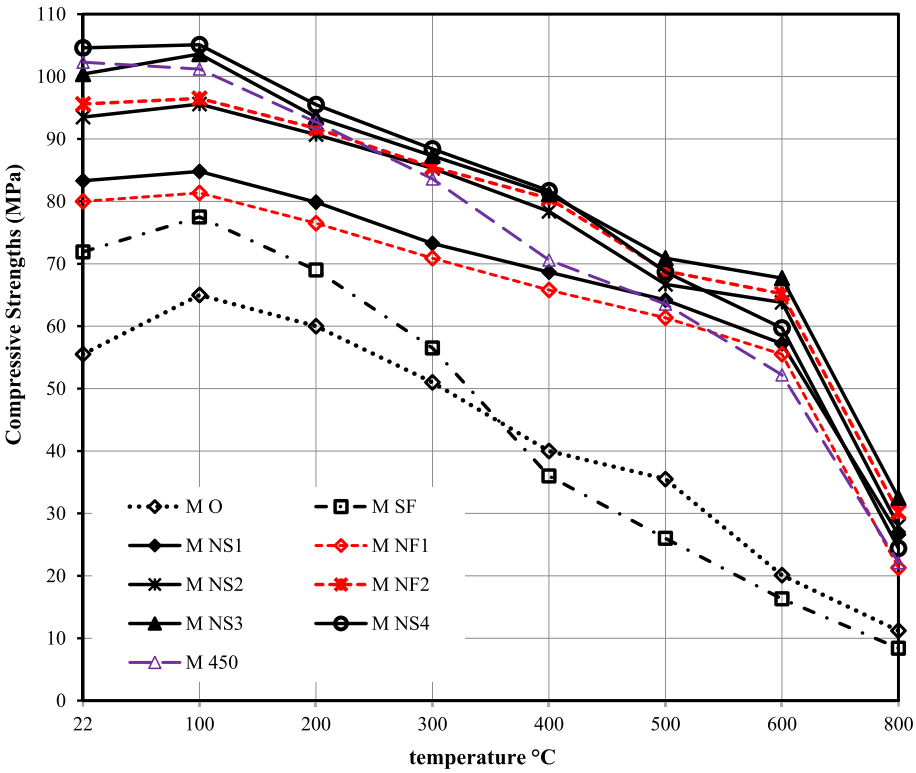

Fig. 11 Compressive strength of concrete mixes at high temperatures up to 800 °C for 2 h

temperatures. The f_c of M_{NF2} was still better than that of M_{NS2} at all temperatures up to 800 °C. At 300 °C, the f_c of M_{NF2} was the best amongst all the M_{NS} mixes, except for M_{NS3} that had the best f_c up to 800 °C.

3.7 SEM analysis of elevated temperature specimens

Figures 12, 13, 14, 15 show SEM images of ITZ between aggregate and CP matrix of M_{SF}, M_{NS2}, M_{NF2} and M_{NS3} mixes at various temperatures (200 °C–800 °C). At 200 °C, SEM image of M_{SF} specimen shows shrinkage of cement paste, emergence of micro-cracks and weakened ITZ due to the chemical and physical loss of water and the decomposition of ettringite. On the contrary, SEM images from specimens of all mixes with nanoparticles show that the cement paste has become denser than before due to the accelerated rate of hydration that formed additional hydration products, especially CAH [41]. This may be due to low thermal conductivity of nanoparticles that delayed the heat transfer of concrete incorporating nanoparticles compared with the heat transfer of normal concrete [42].

At 400 °C, SEM of M_{SF} shows that CH and CSH gel starts to decamp and completely lose water leaving some

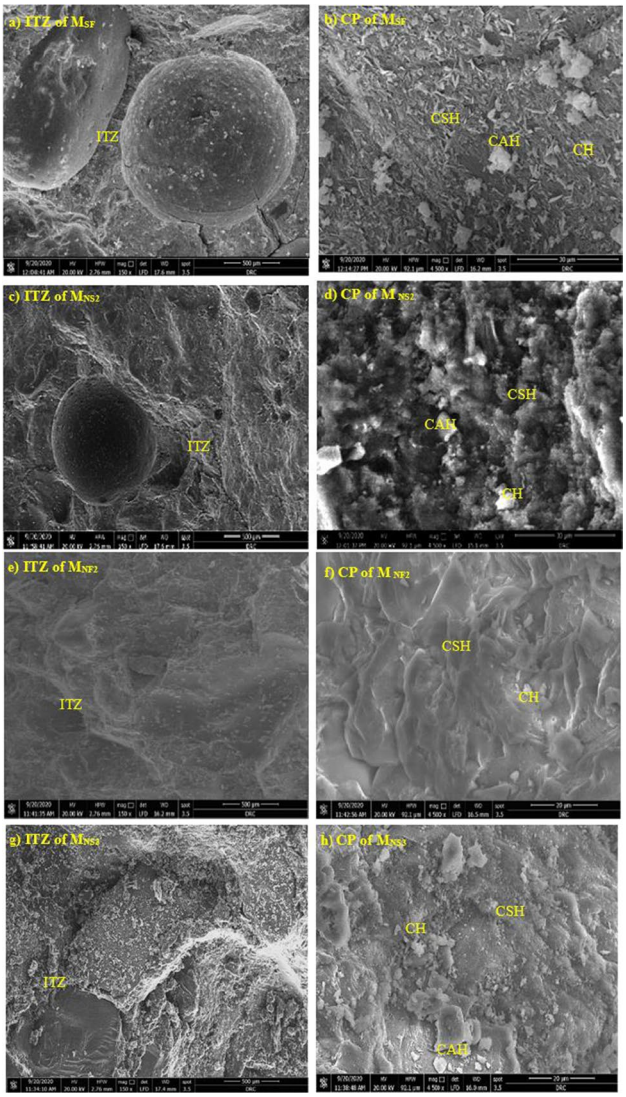

Fig. 12 SEM of ITZ and CP of the mixes at 200 °C

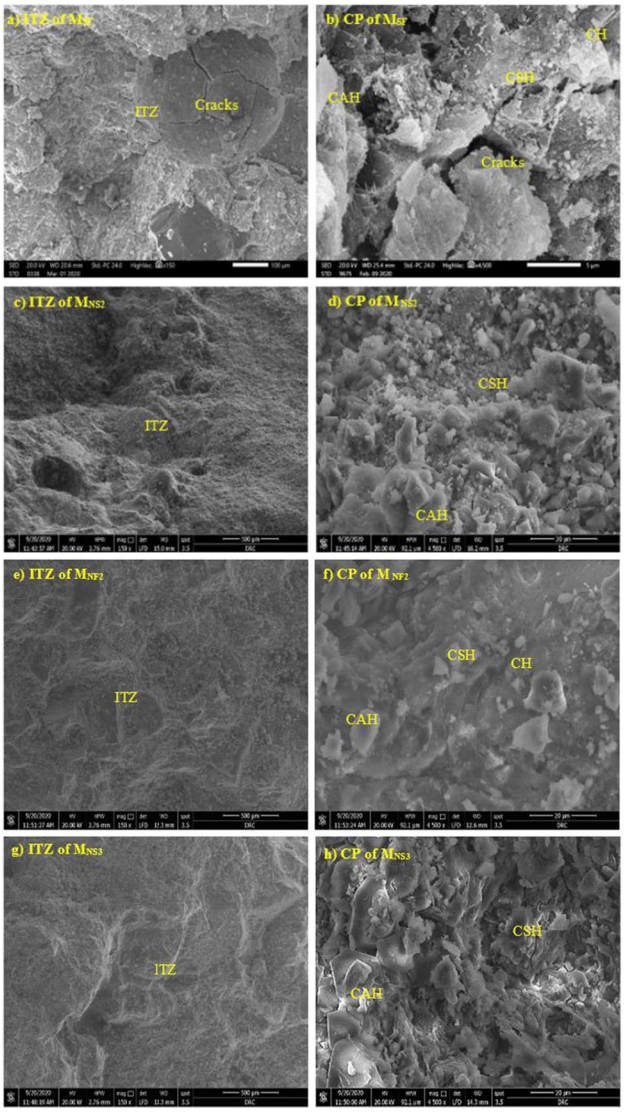

Fig. 13 SEM of ITZ and CP of the mixes at 400 °C

pores in ITZ and a significant increase in micro-cracks are also observed. Extra CAH (as a result of the hydration process) appears in the nanoparticles mix specimens and increases with the increase in nano-particles percentage. At 600 °C, more decomposition of CSH and complete decomposition of CH occur in M_{SF} specimen along with widening of micro-cracks and pores. Micro-cracks begin to appear in M_{NS2} specimen, but no cracks or pores emerge in M_{NF2} and M_{NS3} specimens. Extra CAH is also observed in their specimens. At 800 °C, M_{SF} specimen shows fragmentation, severe cracking, ITZ cracks and loss of bonding due to the disappearance of CSH in the specimen. The number of cracks increase in M_{NS2} specimen but M_{NF2} and M_{NS3} specimens have no cracks up to 800 °C, but their porosity increases slightly.

The fraction surface of the nano-particles mixes is smooth and passed through the aggregate at all temperatures up to 600 °C. SEM images at all temperatures of M_{NS3} and M_{NF2} specimens show that they still have dense matrix without significant cracks due the increment of CSH and CAH and getting rid of CH [23].

3.8 Fire in the presence of initial cracking load

Figure 16 shows the failure compressive strengths of the NS and NF mixes exposed to fire at 600 °C under an initial cracking load of M_o. The strengths were tested at 28 days of age. They were compared with strength of M_o under the same conditions. The results showed that the strengths of the M_o and M_{SF} mixes were 36 and 37.3 MPa, respectively.

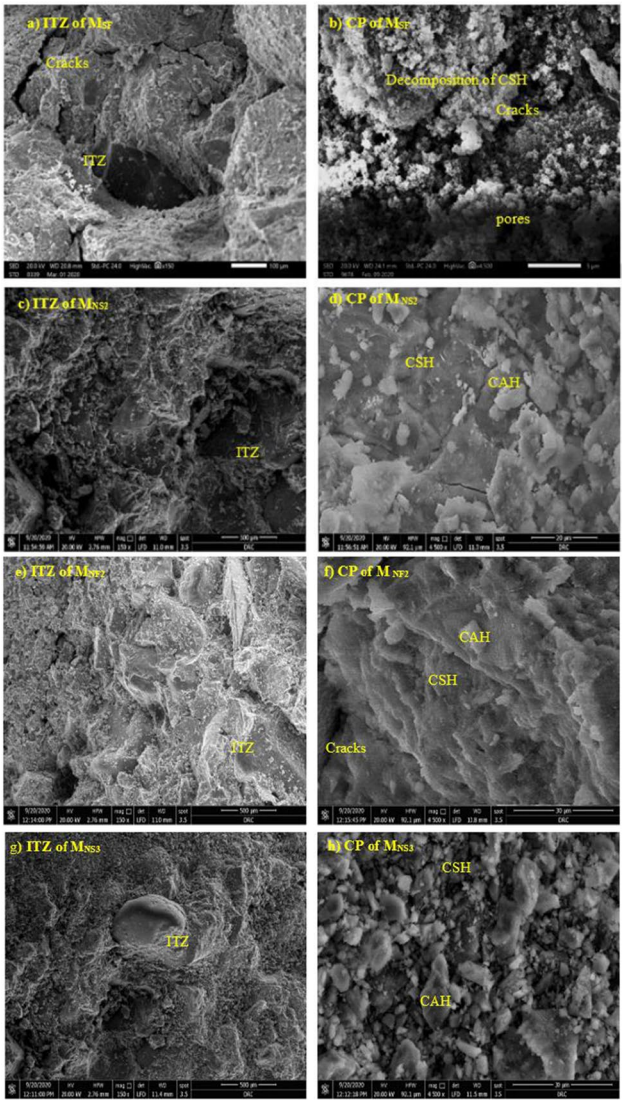

Fig. 14 SEM of ITZ and CP of the mixes at 600 °C

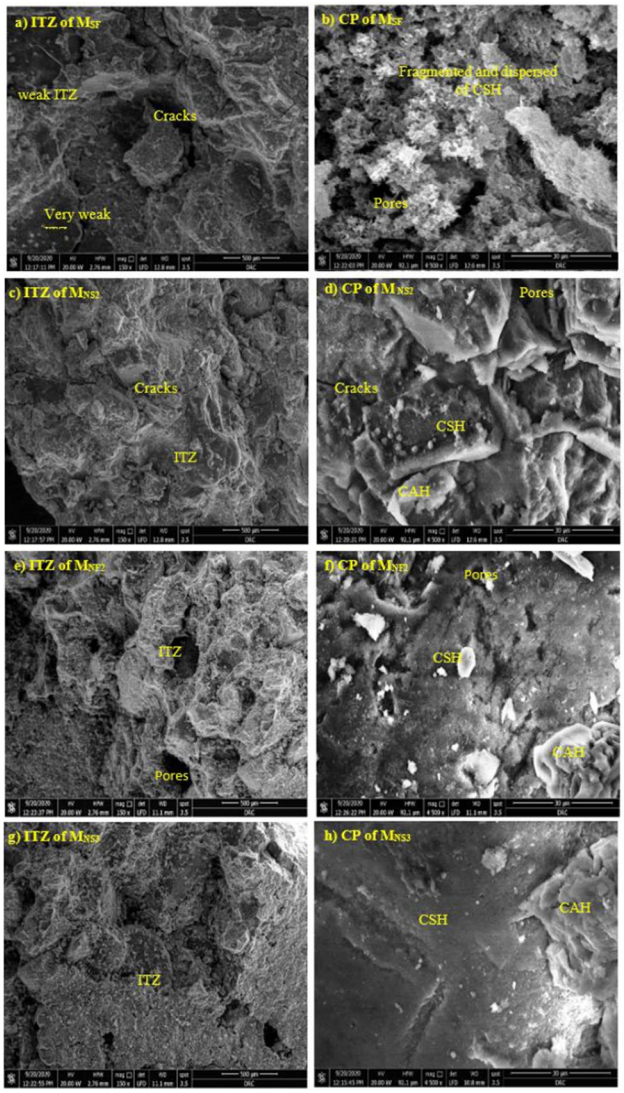

Fig. 15 SEM of ITZ and CP of the mixes at 800 °C

The addition of SF did not improve the residual strength. Residual strength losses were even observed for the same compositions. These results agree with those of Lubloy et al., where the fire-under-load results of NS and NF were almost similar to that of high-temperature exposure results at 600 °C. [43]. For instance, adding NS has improved the fired strength progressively by up to 117% at 3% NS. However, further increasing the NS percentage (MNS4) or the cement content (M450) has reduced the strength improvement to 101.4% and 85% respectively. Thus, M_{NS3} was the best fire resistance mix because it could enhance the mechanical and durability properties of concrete, similar to the conclusions and the fire test results matched with those of Abhilash et al. [44] on exposure to a high temperature of 600 °C.

4 Conclusions

This study analysed the compressive strength of SF mixes with a small content of nanomaterials under exposure to high temperatures and fire in the presence of an initial cracking load. The results of all tested mixes were compared to control mix, M_O. The following conclusions were obtained.

1. At room temperature, the addition of NS can improve the f_c by up to 45.5%.
2. Increasing the cement content of the concrete with 3% NS does not enhance the resistance to high temperatures and fire.
3. The concrete mix with M_{NS4} has demonstrated the lowest relative economic index of the column area, and M_{450}

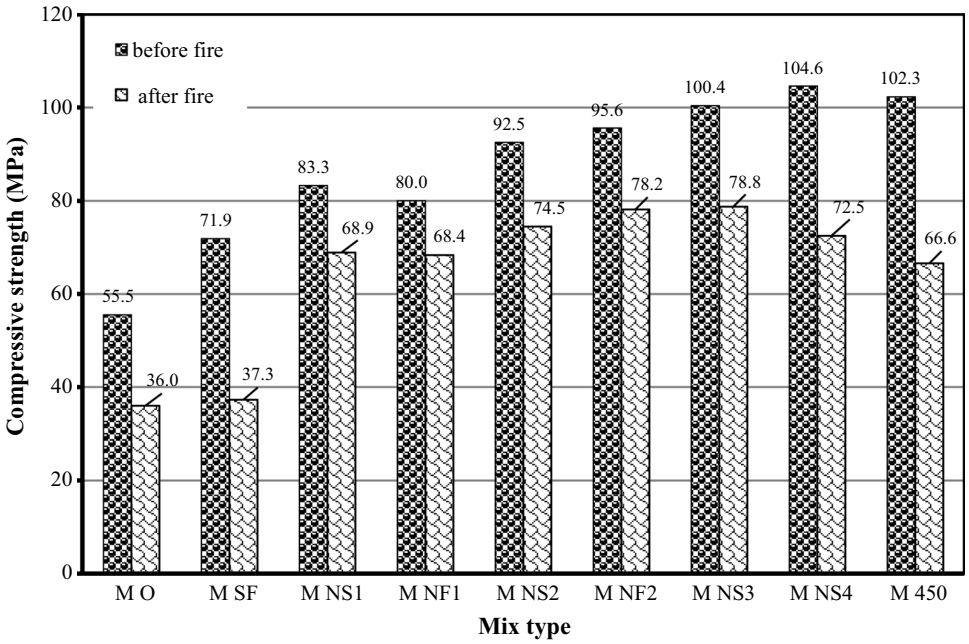

Fig. 16 Compressive strengths of the concrete mixes after fire at 600 °C for 1 h

is the largest relative area reduction with respect to the control mix column area.

4. The addition of 4% NS can enhance the compressive strength by approximately 104% under elevated temperature up to 400 °C.
5. Using 3% NS has demonstrated the best results since the compressive strength under elevated temperatures has improved by up to 230%.
6. The mixes with nanomaterials have demonstrated the best compressive strengths which correspond of the SEM image results.
7. The water permeability of 4% NS has the best reduction percentage reaching to 72%. The K of 2% NF was smaller than that of 2% NS that reached 55.5% and 54.1%, respectively.
8. M_{NS3} had the largest fc amongst the fired concrete specimens in the presence of initial cracking load at 600 °C. Its addition improved the strength of the M_o mix by 117%.

Funding No funding was provided during this research.

Data availability Data can be provided by demand from the corresponding author.

Declarations

Conflict of interest All authors claim that they have no conflict of interest.

References

1. Tawfik TA, Metwally KA, El-Beshlawy S, Al Saffar DM, Hassan HS. Exploitation of the nanowaste ceramic incorporated with nano silica to improve concrete properties. J King Saud Univers Eng Sci. 2021;33(8):581–8.
2. Zeyad AM, Johari MAM, Alharbi YR, Abadel AA, Amran YM, Abutaleb A. Influence of steam curing regimes on the properties of ultrafine pofa-based high-strength green concrete. J Build Eng. 2021;38:102204.
3. Zeyad AM, Johari MAM, Abutaleb A. The effect of steam curing regimes on the chloride resistance and pore size of high–strength green concrete. Constr Build Mater. 2021;280:122409.
4. Hamada H, Yahaya F, Muthusamy K, Al-Attar A. Effects of nano-palm oil fuel ash and nano-eggshell powder on concrete. Construct Build Mater. 2020;261:119790.
5. Alaloul WS, Musarat MA, Sivalingam S, Rosli MFB, Haruna S, Khan MI. Mechanical and deformation properties of rubberized engineered cementitious composite (ecc). Case Stud Constr Mater. 2020;13:e00385.
6. Amin M, Zeyad AM, Agwa IS. Effects of nano cotton stalk and palm leaf ashes on ultrahigh-performance concrete properties incorporating recycled concrete aggregates. Construct Build Mater. 2021;302:124196.
7. Shahidan S, Tayeh BA, Jamaludin AA, Bahari NA, Mohd SS, Ali NZ, Khalid FS. Physical and mechanical properties of self-compacting concrete containing superplasticizer and metakaolin. InIOP Conference Series: Materials Science and Engineering 2017 (Vol. 271, No. 1, p. 012004). IOP Publishing
8. Amin M, Agwa IS. Effect of using mineral admixtures and ceramic wastes as coarse aggregates on properties of ultrahigh-performance concrete. J Clean Prod. 2020;273:123073.
9. Tobbala DE. Effect of nano-ferrite addition on mechanical properties and gamma ray attenuation coefficient of steel fiber reinforced heavy weight concrete. Constr Build Mater. 2019;207:48–58.
10. Janković K, Bojović D, Stojanović M. Influence of nanoparticles on the strength of ultra-high performance concrete. In:

Nanotechnology in eco-efficient construction Pacheco-Torgal F, Diamanti MV, Nazari A, Granqvist CG, Pruna A, Amirkhanian S (Editors), 2019 (pp. 13-42). Woodhead Publishing
11. Sumesh M, Alengaram UJ, Jumaat MZ, Mo KH, Alnahhal MF. Incorporation of nano-materials in cement composite and geopolymer based paste and mortar - a review. Constr Build Mater. 2017;148:62–84.
12. Li H, Xiao H-G, Yuan J, Ou J. Microstructure of cement mortar with nano-particles. Compos B Eng. 2004;35(2):185–9.
13. Li H, Zhang M-H, Ou J-P. Abrasion resistance of concrete containing nano-particles for pavement. Wear. 2006;260(11–12):1262–6.
14. Schoepfer J, Maji A. An investigation into the effect of silicon dioxide particle size on the strength of concrete. Am Concr inst ACI Special Publication. 2009;267:45–58.
15. Faried AS, Mostafa SA, Tawfik TA. The effect of using nano rice husk ash of different burning degrees on ultra-high-performance concrete properties. Constr Build Mater. 2021;290:123279.
16. Mechanical and durability properties of ultra-high performance concrete incorporated with various nano waste materials under different curing conditions. J Build Eng 2021;43:102569.
17. Tayeh BA, Hasaniyah MW, Zeyad AM, Awad MM, Alaskar A, Mohamed AM, Alyousef R. Durability and mechanical properties of seashell partially-replaced cement. J Build Eng. 2020;31:101328.
18. Kumar R, Singh S, Singh LP. Studies on enhanced thermally stable high strength concrete incorporating silica nanoparticles. Constr Build Mater. 2017;153:506–13.
19. Amin M, Gamal SMA, Hashem F. Effect of addition of nano-magnetite on the hydration characteristics of hardened Portland cement and high slag cement pastes. J Therm Anal Calor. 2012;112:1253–9.
20. Amin M, Tayeh BA. Investigating the mechanical and microstructure properties of fibre-reinforced lightweight concrete under elevated temperatures. Case Stud Constr Mater. 2020;13: e00459.
21. Elsayed M, Abou Elmaaty M, Aldahshoory Y. Behaviour of rc columns strengthened with ultra-high performance fiber reinforced concrete (uhpfrc) under eccentric loading. J Build Eng. 2022;47:103857.
22. Amin M, Zeyad AM, Tayeh BA, Agwa IS. Effect of ferrosilicon and silica fume on mechanical, durability, and microstructure characteristics of ultra high-performance concrete. Constr Build Mater. 2022;320:126233.
23. Tobbala DE, Abdelsalam BA, Agwa IS. Bond performance of a hybrid coating zinc-rich epoxy incorporating nano-ferrite for steel rebars subjected to high temperatures in concrete. J Build Eng. 2020;32:101698.
24. Bastami M, Baghbadrani M, Aslani F. Performance of nano-silica modified high strength concrete at elevated temperatures. Constr Build Mater. 2014;68:402–8.
25. Abdul-Rahman M, Al-Attar AA, Hamada HM, Tayeh B. Microstructure and structural analysis of polypropylene fibre reinforced reactive powder concrete beams exposed to elevated temperature. J Build Eng. 2020;29:101167.
26. Al-Attar AA, Abdulrahman MB, Hamada HM, Tayeh BA. Investigating the behaviour of hybrid fibre-reinforced reactive powder concrete beams after exposure to elevated temperatures. J Mater Res Technol. 2020;9:1966–77.
27. Yonggui W, Shuaipeng L, Hughes P, Yuhui F. Mechanical properties and microstructure of basalt fibre and nano-silica reinforced recycled concrete after exposure to elevated temperatures. Constr Build Mater. 2020;247:118561.
28. Al Saffar DM, Tawfik TA, Tayeh BA. Stability of glassy concrete under elevated temperatures. Eur J Environm Civil Eng. 2021;26:1–12.
29. Haido JH, Tayeh BA, Majeed SS, Karpuzcu M. Effect of high temperature on the mechanical properties of basalt fibre self-compacting concrete as an overlay material. Constr Build Mater. 2021;268:121725.
30. Tayeh BA, Zeyad AM, Agwa IS, Amin M. Effect of elevated temperatures on mechanical properties of lightweight geopolymer concrete. Case Stud Constr Mater. 2021;15: e00673.
31. Abed MA, Tayeh BA, Abu Bakar B, Nemes R. Two-year non-destructive evaluation of eco-efficient concrete at ambient temperature and after freeze-thaw cycles. Sustainability. 2021;13:10605.
32. Ramadan M, Amin M, Sayed MA. Superior physico-mechanical, fire resistivity, morphological characteristics and gamma radiation shielding of hardened opc pastes incorporating znfe2o4 spinel nanoparticles. Constr Build Mater. 2020;234:117807.
33. Ibrahim RK, Hamid R, Taha MR. Fire resistance of high-volume fly ash mortars with nanosilica addition. Constr Build Mater. 2012;36:779–86.
34. Ramadan M, Amin MS, Sayed MA. Superior physico-mechanical, fire resistivity, morphological characteristics and gamma radiation shielding of hardened opc pastes incorporating znfe2o4 spinel nanoparticles. Constr Build Mater. 2020;234:117807.
35. El-Enein SAA, Kishar EA, Zedan SR, Mohamed RA. Effect of nano-sio2 (ns) on dolomite concrete towards alkali silica reaction. HBRC J. 2018;14(2):165–70.
36. Nili M, Ehsani A. Investigating the effect of the cement paste and transition zone on strength development of concrete containing nanosilica and silica fume. Mater Des. 2015;75:174–83.
37. Ahmed MA, Ahmed SA, Metwally ME, Sherif MA, Tobbala DE Preparation of nano-silica from rice husk ash using acid chemical treatment and burning. The International Conference of Engineering Sciences and Applications, Aswan, Egypt, 2016
38. ASTM, C143/ and C143M-15a, "Standard test method for slump of hydraulic-cement concrete," ASTM International, West Conshohocken, PA 2015.
39. ASTM, C33 and C33M-18, "Standard specification for concrete aggregates," ASTM International, West Conshohocken, PA, 2018.
40. ASTM, Standard test methods for fire tests of building construction and materials, ASTM International, West Conshohocken, PA., 2000.
41. Abhilash PP, Nayak DK, Sangoju B, Kumar R, Kumar V. Effect of nano-silica in concrete; a review. Constr Build Mater. 2021;278:122347.
42. Heikal M, El-Didamony H, Sokkary TM, Ahmed IA. Behavior of composite cement pastes containing microsilica and fly ash at elevated temperature. Constr Build Mater. 2013;38:1180–90.
43. Lubloy E, Balazs GL, Czoboly O, Harman B Influence of silica fume on fire resistance. 2011:305–308.
44. Abhilash PP, Nayak DK, Sangoju B, Kumar R, Kumar V. Effect of nano-silica in concrete; a review. Constr Build Mater. 2021;278:122347.

Publisher's Note Springer Nature remains neutral with regard to jurisdictional claims in published maps and institutional affiliations.